

## Diffusive-Flux-Driven Microturbines by Fore-and-Aft Asymmetric Phoresis

Mingren Shen,<sup>1,2,3</sup> Rui Liu,<sup>1</sup> Ke Chen,<sup>1,2,\*</sup> and Mingcheng Yang<sup>1,2,†</sup>

<sup>1</sup> Beijing National Laboratory for Condensed Matter Physics and Key Laboratory of Soft Matter Physics, Institute of Physics, Chinese Academy of Sciences, Beijing 100190, China

<sup>2</sup> School of Physical Sciences, University of Chinese Academy of Sciences, Beijing 100049, China

<sup>3</sup> Department of Materials Science and Engineering, University of Wisconsin-Madison, Madison, Wisconsin 53706, USA

(Received 13 February 2019; revised manuscript received 13 August 2019; published 25 September 2019)

A turbine can convert translational kinetic energy of convective flows into rotation and is one of the most important machines to harvest energy from nature. Here, we propose a theoretical prototype of a micro-turbine that is powered purely by an external diffusive heat or mass flux. The turbine rotates perpendicular to the external thermal or chemical gradient due to fore-and-aft asymmetric thermophoresis or diffusiophoresis. Thus, its performance does not need alignment. The prototype turbine is validated by means of computer simulations. The results show that the angular velocity of the turbine sensitively depends on its structure and interactions with the solvent. This perpendicular-axis phoretic turbine provides large flexibility and the possibility to exploit existing thermal or chemical energies at small scales.

DOI: 10.1103/PhysRevApplied.12.034051

### I. INTRODUCTION

Turbines can extract mechanical work from convective flows and are often used to harvest energy from nature. Most turbines operate on macroscopic scales, including wind turbines, hydraulic turbines, or steam turbines. Light-driven microturbines have also been developed recently [1–4]. The common principle of such turbines is to utilize a nonsymmetric structure to convert the momentum of a convective flow into rotational torque. Besides convective flows, diffusive fluxes also carry exploitable energy, including heat fluxes from temperature gradients or mass fluxes from concentration gradients. Such diffusive fluxes are ubiquitous on small scales, from thermal gradients in microelectric chips to chemical gradients in microfluidics. In the presence of a thermal or chemical gradient, mesoscopic particles, such as colloids, exhibit directed motion in the gradient field; this phenomenon is known as phoresis [5–9]. Our recent theoretical work [10,11] led to the design of microturbines powered by a diffusive (heat or mass) flux based on anisotropic phoresis [12]. These phoretic microturbines are in fundamental contrast to traditional turbines. The phoretic microturbines are able to exploit heat and chemical energies from external temperature and concentration gradients, which would be otherwise wasted through heat conduction or mass diffusion.

In external gradient fields, the diffusive-flux-driven turbines proposed previously are subjected to a phoretic torque parallel to the gradient and unidirectionally rotate along the diffusive flux [10,11]. On the other hand, for convective flow-driven turbines, the rotational direction can also be designed to be perpendicular to the flow direction, e.g., the Darrieus wind turbine [13,14] and waterwheel. This provides more choice and additional advantages for practical applications. In line with the apparent similarity between convective and diffusive turbines, it is interesting and desired to investigate the possibility of phoretic turbines with their rotational direction perpendicular to that of external diffusive flows.

Here, we present a design for both thermophoretic and diffusiophoretic microscale turbines that can spontaneously and unidirectionally rotate perpendicular to external diffusive heat and mass fluxes, respectively. The proposed diffusive turbines consist of microscale blades with fore-and-aft nonsymmetric phoretic effects. This phoretic asymmetry can induce a driving phoretic torque perpendicular to the external thermal or chemical gradient on the turbines. The feasibility of this type of perpendicular-axis phoretic turbines is justified by performing mesoscale dynamics simulations. The obtained results are consistent with symmetry analyses.

### II. MODEL AND SIMULATION METHOD

For simplicity, we consider a 2D turbine system (Fig. 1). The turbine is composed of three blades connected to the turbine center by rigid bonds of length  $L$  (geometric

\*kechen@iphy.ac.cn

†mcyang@iphy.ac.cn

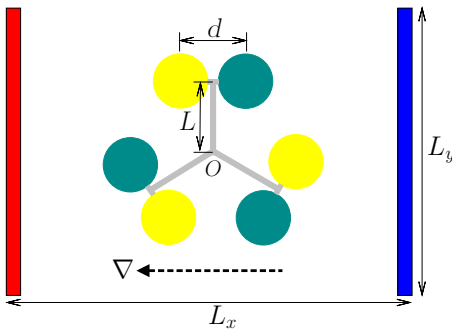


FIG. 1. Schematic diagram of a microscale turbine consisting of three dumbbell particles, which are connected by rigid bonds (gray) and form a rigid body. The included angle between two bonds is  $2\pi/3$ . The turbine center (O) is fixed in the middle of the system. The fluid particles are not drawn explicitly.

constraint). The turbine is allowed to rotate freely around its center, which is fixed in a solution. Each blade is a dumbbell consisting of two beads (I and II), separated by a distance of  $d$ . To achieve a phoretic turbine that spontaneously and unidirectionally rotates perpendicular to the gradient, the following three symmetries have to be broken. The first one is time-reversal symmetry, which is intrinsically broken because of the gradient-induced nonequilibrium state. The second symmetry that needs to be broken is mirror reflection through a plane containing the rotational axis, since, otherwise, the turbine and its mirror image have the same rotational direction, which means no net rotation. For example, a general hexagonal turbine with identical blade beads is mirror-reflection symmetric with respect to the plane formed by the rotational axis and any rigid bond. Due to symmetry, such a turbine is stable when a rigid bond is parallel to the gradient field. The third one is fore-and-aft symmetry of the phoresis of the blade, that is, reversal of the blade does not affect the phoretic force upon it. This requirement can be understood by noting that reversal of the turbine blades leads to opposite rotation of the turbine, such that the rotational velocity must be vanishing if the blade phoresis is fore-and-aft symmetric. Therefore, asymmetric phoresis is critical for building perpendicular-axis phoretic turbines and it is explained in detail as follows. Notably, the third symmetry does not imply the second one, since a regular hexagonal turbine with different blade beads [see Fig. 4(c)] clearly breaks the third symmetry, but still meets the mirror-reflection symmetry.

### A. Fore-and-aft asymmetric phoresis

In solutions with thermal or chemical gradients,  $\nabla\Psi$ , suspended particles can be subjected to a driving force, and hence, drift along or against the gradients; these phenomena are often referred to as thermophoresis [6,7,15–19] or diffusiophoresis [8,20–23], respectively. Phoretic

effects have been widely used to manipulate mesoscale particles [24–30] and to design active colloids [31–33]. For an isotropic particle, the phoretic force depends on the gradient by  $\mathbf{f}_p = \alpha\nabla\Psi$ , with a scalar prefactor,  $\alpha$  [5–8]. For instance, in the case of thermophoresis,  $\nabla\Psi = \nabla T$  and  $\alpha = -\alpha_T k_B$ , in which  $k_B$  is the Boltzmann constant,  $\alpha_T = TS_T$  is the thermodiffusion factor, and  $S_T$  is the Soret coefficient [6,34]. For diffusiophoresis,  $\nabla\Psi = \nabla c$  and  $\alpha = \alpha_D = \gamma D_{DP}/c$ , in which  $\gamma$  and  $D_{DP}$  refer to the frictional coefficient and diffusiophoretic mobility, respectively [20,21]. Generally, for an anisotropic particle with nonsymmetric geometry or nonuniform material, the phoretic factors will have different components, and scalar  $\alpha$  is then replaced by a tensorial prefactor, namely,  $\mathbf{f}_p = \Lambda \cdot \nabla\Psi$ . Here, the elements of  $\Lambda$  may generally depend on the orientation of the particle.

Previous studies [10–12] have shown that the phoresis of a homogeneous rodlike particle can be described by two independent factors, which correspond to phoretic factors along the long and short axes of the particle. Due to this anisotropy, the phoretic force on the particle may have a component perpendicular to  $\nabla\Psi$ , by which one can design diffusive-flux-driven turbines rotating parallel to the gradient.

Now, we consider a colloidal dumbbell consisting of different beads, I and II [Fig. 2(a)]. It is expected that such a particle suffers from different phoretic forces with its fore ( $n_+$ ) or rear ( $n_-$ ) ends toward  $\nabla\Psi$  [Fig. 2(a)], since the local environments felt by the particle in the two configurations are different. Specifically, the phoretic force not only depends on the field gradient, but also on local solute concentration [5,35–37] or temperature [38,39] via the phoretic factor. This dependence of the phoretic factor

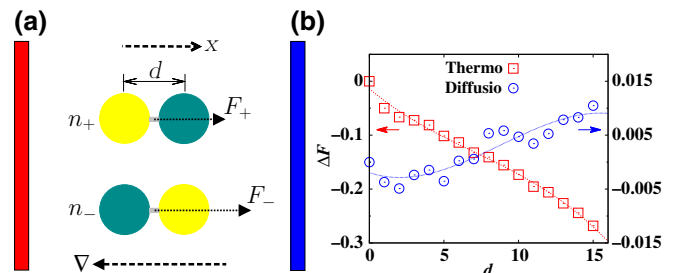


FIG. 2. (a) Schematic diagram of an asymmetric dumbbell fixed in a solution with a thermal or chemical gradient. The yellow and cyan beads refer to bead I (fore end of the dumbbell) and bead II (rear end), respectively. The left red wall represents a high-temperature or high-concentration wall. The phoretic forces on the dumbbell of configurations  $n_+$  and  $n_-$  are  $F_+$  and  $F_-$ , respectively. (b) The phoretic force differences as a function of bead separation. Squares and circles correspond to thermophoretic (with  $\nabla T \simeq -0.0167$ ) and diffusiophoretic (with the concentration gradient of species B,  $\nabla c \simeq -0.088$ ) cases, respectively. Lines are used to guide the eye.

on local concentration or temperature is critical for breaking the fore-and-aft symmetry of phoresis of the dumbbell. Although the centers of the dumbbell for configurations  $n_+$  and  $n_-$  are identical, the local physical conditions encountered by beads I and II of the dumbbell are swapped. This results in a change of the phoretic force on the dumbbell. Note that the breaking of fore-and-aft symmetry for phoresis is related to, but not equivalent to, phoretically asymmetric particles (e.g., partially coating Janus particles), the constituent materials of which on the two sides have heterogeneous phoresis. That is, a Janus particle with heterogeneous material does not necessarily exhibit fore-and-aft nonsymmetric phoresis.

Using this anisotropic dumbbell as the blade, we can construct a turbinelike structure (see Fig. 1). In a gradient field, such a turbine is expected to rotate perpendicular to the gradient, as it meets all the required asymmetries for unidirectional rotations discussed above. Therefore, we expect that the turbinelike structure experiences a nonzero phoretic torque perpendicular to the gradient, and hence, rotates around its fixed center. To verify the feasibility of the designed turbine, we use a hybrid mesoscale simulation scheme to bridge the gap in characteristic time and length between the solvent molecules and the turbine. Here, the fluid is simulated by multiparticle collision dynamics (MPC) [40–43], while the turbine is described by standard molecular dynamics (MD).

### B. MPC fluid

In MPC, the solvent is modeled as  $N$  pointlike particles of mass  $m$ , with continuous positions  $\mathbf{r}_i(t)$  and velocities  $\mathbf{v}_i(t)$ . The particle dynamics consists of alternating streaming and collision steps. In the streaming step, all solvent particles move ballistically for time  $h$ . In the collision step, particles are sorted into a square lattice with lattice size  $a$ , and interchange momentum relative to the center-of-mass velocity of each collision cell. In our simulations, the stochastic rotation collision rule with variable collision angle  $\alpha$ , introduced by Ryder and Yeomans [43,44], is employed. This collision rule locally conserves mass, linear momentum, energy, and angular momentum. Thus, the algorithm can properly capture hydrodynamics, thermal fluctuations, thermal conduction, mass diffusion, and dissipation. Simulation units are reduced by setting  $a = 1$ ,  $m = 1$ , and the system mean temperature to  $k_B\bar{T} = 1.0$ . From the basic MPC units, the time unit is  $a\sqrt{m/k_B\bar{T}}$ , such that the unit for angular velocity is  $(a\sqrt{m/k_B\bar{T}})^{-1}$ . In the simulations, we employ  $h = 0.1$  and the mean number of solvent particles per cell  $\rho = 10$ .

Unless otherwise stated, the simulation box is a square of dimensions  $L_x = L_y = 48$ , with nonslip boundary walls [45] in the  $x$  direction and periodic boundary conditions in the  $y$  direction. The external gradient field is applied in the  $x$  direction. In the case of the thermophoretic

turbine, the temperature gradient is established by thermostating thin fluid layers close to the left and right walls with different temperatures. This boundary thermostat [46–49] ensures that heat conduction can be correctly accounted for inside the system. In the diffusiophoretic case, the MPC fluid is a binary mixture consisting of equimolar species A and B. These two species couple to each other via MPC collisions and are only distinguishable in their collisions with the turbine [50,51]. The stationary chemical gradient is produced by fixing the molar fraction of B-type fluid particles near the two walls to different values [11], which are easily obtained by changing the particle species accordingly. The boundary operation for establishing a chemical gradient is equivalent to a system connected to two reservoirs with different concentrations and ensures that mass diffusion is physically correct inside the solution.

### C. Microscale turbine

In the simulations,  $L$  and  $d$  (Fig. 1) are varied to achieve different turbine structures. The beads interact with the solvent particles through Lennard-Jones (LJ) type potential

$$U(r) = 4\epsilon \left[ \left( \frac{\sigma}{r} \right)^{2n} - \left( \frac{\sigma}{r} \right)^n \right] + c \quad r \leq r_c.$$

Here,  $r$  refers to the distance from the bead center to the solvent particle,  $\epsilon$  to the potential intensity,  $\sigma$  to the bead radius,  $n$  to a positive integer describing the potential stiffness, and  $r_c$  to the cutoff distance. By considering  $c = \epsilon$  or  $c = 0$  together with the corresponding  $r_c$ , the potential can be purely repulsive or have an attractive tail. Throughout,  $\sigma = 3$  and  $\epsilon = 1$  are used, and  $n$  is varied. For convenience, the notations  $\text{rep}(n)$  and  $\text{att}(n)$  are used to represent the repulsive and attractive LJ potentials, respectively, with a prescribed  $n$ . To model fore-and-aft asymmetry, the two beads of the blade have different interactions with the solvent, which are separately denoted as  $U_I$  and  $U_{II}$ . The mass of the bead is set to  $M = \pi\sigma^2\rho m$ , such that the turbine is neutrally buoyant. The equations of motion of the turbine and its neighbouring solvent are integrated by the velocity Verlet algorithm with a time step  $\Delta t = h/50$ .

## III. RESULTS

### A. Dumbbell blade

Before simulating the phoretic turbines, we check whether the nonsymmetric dumbbell has fore-and-aft asymmetric phoresis. For this purpose, we directly measure the phoretic forces on the dumbbell fixed with configurations  $n_+$  and  $n_-$  [Fig. 2(a)], namely,  $F_+$  and  $F_-$ , respectively. To enhance the asymmetry of the dumbbell, the interactions of the two beads with the solvent are chosen in such a way that the two beads experience opposite phoretic forces. For the thermophoretic dumbbell, we take  $U_I = \text{att}(30)$  and  $U_{II} = \text{rep}(3)$ , such that

beads I and II are separately thermophobic or thermophilic [52,53]. While, for the diffusiophoretic blade, we take  $U_{I,A} = U_{II,A} = \text{rep}(24)$ ,  $U_{I,B} = \text{att}(30)$  and  $U_{II,B} = \text{rep}(3)$ , where the subscript,  $A$  or  $B$ , denotes the solvent component. As a consequence, the diffusiophoretic forces exerted on beads I and II are, respectively, along and against the concentration gradient of species B [50,51].

Figure 2(b) plots the force difference,  $\Delta F = F_+ - F_-$ , as a function of  $d$ , which shows that the phoresis of the dumbbell is indeed fore-and-aft nonsymmetric. Nonvanishing  $\Delta F$  arises from the fact that dumbbells  $n_+$  and  $n_-$  are not equivalent in the gradients, as explained in Sec. II. Unless the dumbbell is symmetric or the gradient is lacking, the phoretic asymmetry generally exists. We are now in the position to investigate the perpendicular-axis phoretic turbines that consist of the asymmetric dumbbell blades (see Fig. 1).

## B. Thermophoretic turbine

The mean rotational angle of a typical thermophoretic turbine in a thermal gradient is plotted in Fig. 3(a). The results show that the turbine indeed unidirectionally rotates perpendicular to  $\nabla T$ . Here, a counterclockwise rotation is defined as positive. Interestingly, the rotational direction is independent of the direction of the thermal gradient. The independence comes from the fact that changing the direction of  $\nabla T$  is simply equivalent to changing the initial angle of the turbine relative to the  $x$  axis (see Fig. 1), and thus, does not affect the rotational direction. The perpendicular-axis turbine shares the same features as those of the Darrieus wind turbine, the performance of which does not need an alignment operation. Opposite rotation is achieved by inverting each dumbbell blade with respect to its center [Fig. 3(a)]. If  $\nabla T = 0$ , no net rotation occurs. Figure 3(b) plots the angular velocity of the turbine,  $\omega$ , as a function of  $\nabla T$ , which is symmetric about  $\nabla T = 0$ .

Further, we study the geometric effect on turbine performance by systematically tuning  $d$  and  $L$ , as illustrated in Fig. 4. Figure 3(c) shows that the rotational direction and magnitude depend on  $L$  and  $d$ . In particular, the angular velocity exhibits a nonmonotonic dependence on  $d$ , and vanishes for certain configurations [regular hexagon, as in Fig. 4(c), and regular triangle, as in Figs. 4(a) and 4(e)], in which the turbine obeys mirror-reflection symmetry. This agrees with the symmetry analysis presented in Sec. II. The geometric dependence provides flexibility for designing and optimizing the turbine. The driving torque on the turbine could, in principle, be calculated theoretically, once the thermophoretic force on each bead is known. However, because the thermophoretic force varies with the temperature felt by the bead (hence its position) and different beads of the turbine may lead to a correlation effect, a theoretical calculation of the phoretic torque is far from trivial.

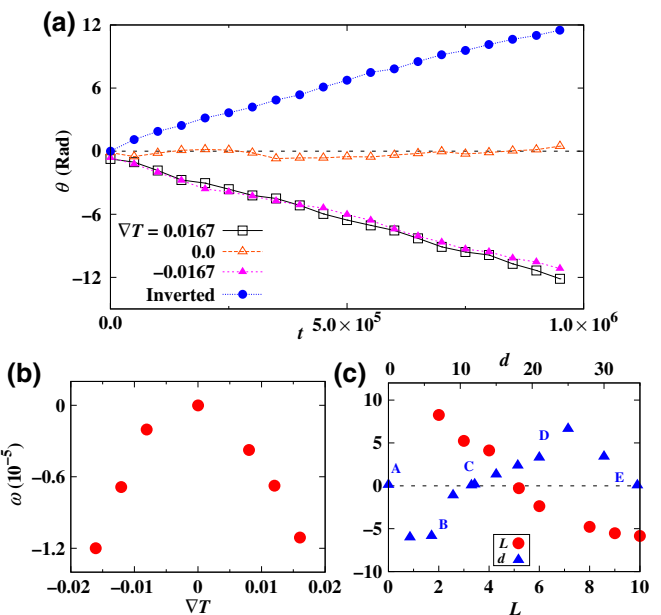


FIG. 3. Rotation of a thermophoretic turbine with  $U_I = \text{att}(30)$  and  $U_{II} = \text{rep}(3)$ . (a) Rotational angle of the turbine versus time. Here, different values of  $\nabla T$  are considered, and “inverted” refers to the turbine with blades inverted relative to that in Fig. 1. (b) Angular velocity of the turbine as a function of temperature gradient. In (a) and (b),  $d = 9$  and  $L = 10$  are used. (c) Angular velocity as a function of  $L$  for  $d = 6$  (bottom horizontal axis, red circle) and of  $d$  for  $L = 10$  (top horizontal axis, blue triangle), with  $\nabla T \simeq -0.0167$ . Here, triangles “A–E” correspond to turbines (a)–(e) in Fig. 4, respectively.

In our 2D systems, finite size effects may be significant, owing to hydrodynamic interactions. We study the finite size effects on the obtained results by performing additional simulations with different system sizes. The angular velocities for different system sizes are summarized in Table I. The results show that the finite size effects are

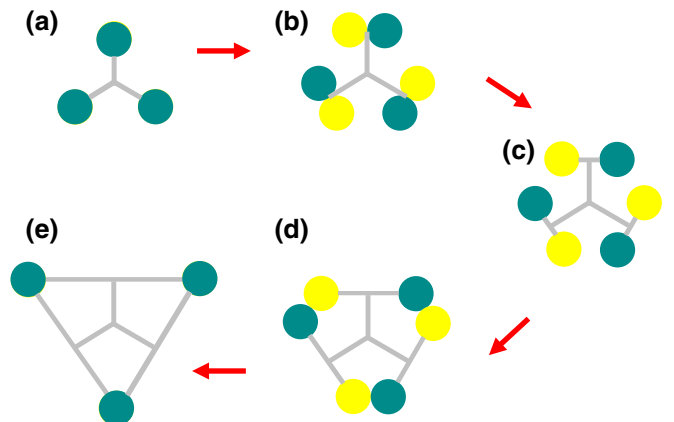


FIG. 4. (a)–(e) Several typical turbine shapes, as realized by changing  $d$  with fixed  $L$ . Turbines in (a) and (e) are regular triangles, and the turbine in (c) is a regular hexagon.

TABLE I. Finite size effects on the angular velocity of the thermophoretic turbine, with  $U_I = \text{att}(30)$ ,  $U_{II} = \text{rep}(3)$ ,  $L = 10$ ,  $d = 6$  and  $\nabla T \simeq 0.0167$ .

$L_x = L_y$	36	48	72	96
$\omega (10^{-5})$	-6.58	-5.85	-5.22	-5.40

not important in our simulations, except for a very small system size. This is because the flow field induced by the rotation of the microturbine is relatively short-range.

Finally, we provide an evaluation of the performance of the thermophoretic turbine under experimental conditions. This can be roughly obtained by mapping the simulation units of the MPC model to those of real physical systems. We employ a similar strategy to that introduced in Refs. [41] and [54], in which the mean simulation temperature,  $\bar{T}$ , is matched to 300 K and the mass density of the MPC solvent to that of water, 1 g/cm<sup>3</sup>. We further consider the radius of the dumbbell bead,  $\sigma = 1 \mu\text{m}$ . From these three parameters, all other physical quantities can be derived, for instance, the size of the collision cell,  $a = 1/3 \mu\text{m}$ ; the mass of a MPC fluid particle,  $m \simeq 4 \times 10^{-18} \text{ kg}$ ; and the simulation time unit,  $a\sqrt{m/k_B T} \simeq 10^{-5} \text{ s}$ . Thus, from Fig. 3(c), the typical angular speed of the thermophoretic turbine is about 3 Rad/s. However, the mesoscopic nature of the MPC solvent makes it impossible to simultaneously match all relevant physical quantities to their realistic values. For example, the mapped solvent viscosity,  $\eta$ , is 100 times smaller than that of water; the mapped  $\nabla T$  is 15 times larger than that of the experimental case; and  $\alpha_T$  of the simulation dumbbell bead is 200 times smaller than that of a polystyrene particle with a radius of 1  $\mu\text{m}$ ,  $\alpha_T^{\text{ps}} \sim 2000$  [39]. To validate the mapped angular speed, we need to analyze all derived quantities that influence the angular speed, i.e.,  $\eta$ ,  $\nabla T$ , and  $\alpha_T$ . Their effects on the turbine angular speed can be given by the ratio of the realistic  $\alpha_T \nabla T / \eta$  to its mapped value, since low  $\eta$  and high  $\nabla T$  result in an overestimation of the angular speed, while small  $\alpha_T$  underestimates the angular speed. With this consideration, the mapped rotational speed is corrected by a factor 0.13, such that  $\omega \sim 0.4 \text{ Rad/s}$ .

In addition to mapping being obtained from the simulations, the realistic rotational speed of the microturbine can also be evaluated by a dimensional argument directly based on experimental quantities. In the steady state, driving and frictional torques on the turbine balance each other,  $\gamma_r \omega = \tau$ , where the driving torque reads  $\tau \simeq \delta \alpha_T k_B \nabla T \sigma$ , in which the prefactor  $\delta \leq 1$  describes the degree of phoretic anisotropy and the rotational frictional coefficient is  $\gamma_r \simeq 4\pi \eta \sigma^3$ . Considering  $\nabla T \simeq 0.2 \text{ K}/\mu\text{m}$  and a moderate phoretic anisotropy  $\delta = 0.2$ , we have  $\omega \sim 0.1 \text{ Rad/s}$  for the thermophoretic turbine with 1  $\mu\text{m}$  blade bead, which is comparable to that obtained from the mapping outlined above.

### C. Diffusiophoretic turbine

After investigating the thermophoretic turbine, we simulate the diffusive mass-flux-driven turbine, and the simulation results are plotted in Fig. 5. As expected, the diffusiophoretic turbine has similar rotational features to that of the thermophoretic one. The diffusiophoretic turbine rotates perpendicular to the external chemical gradient spontaneously and unidirectionally; for a given turbine, changing  $\nabla c$  only affects its rotational speed, rather than its rotational direction [Figs. 5(a) and 5(b)]; and the angular velocity of the turbine significantly depends on its structure [Fig. 5(c)] and vanishes for structures with mirror-reflection symmetry.

Since the diffusiophoretic turbine is driven by non-symmetric diffusiophoresis of the constituent blades, one expects that the angular speed of the turbine is enhanced as the asymmetry of the blade increases. To test this argument, we implement simulations for turbines with different  $U_{I,B}(n)$ . Upon fixing all other parameters, reducing  $n$  of  $U_{I,B}(n)$  increases the range of the attractive potential well, and hence, its effective strength, which increases

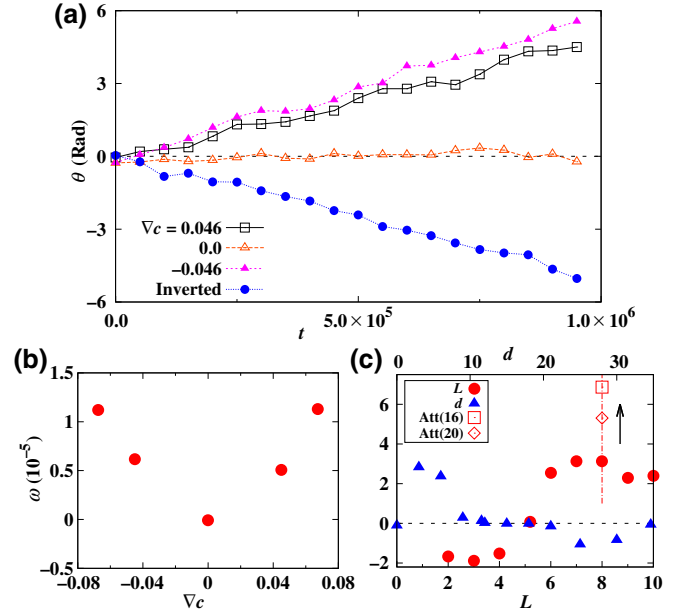


FIG. 5. Rotation of a diffusiophoretic microturbine with  $U_{I,A} = U_{II,A} = \text{rep}(24)$ ,  $U_{I,B} = \text{att}(30)$ , and  $U_{II,B} = \text{rep}(3)$ . (a) Rotational angle of the turbine versus time. Here, different values of  $\nabla c$  are used, and “inverted” refers to the turbine with blades inverted relative to that in Fig. 1. (b) Angular velocity of turbine as a function of the concentration gradient of species B. In (a) and (b),  $d = 6$  and  $L = 10$  are used. (c) Angular velocity as a function of  $L$  for  $d = 6$  (red circle, bottom horizontal axis) and of  $d$  for  $L = 10$  (blue triangle, top horizontal axis), with  $\nabla c \simeq -0.088$ . The open diamond and square correspond to turbines with  $U_{I,B} = \text{att}(20)$  and  $\text{att}(16)$ , respectively, in which  $d = 6$  and  $L = 8$ . Vertical line and arrow are used to guide the eye.

the asymmetry of the blade. The simulation results [see the symbols on the longitudinal red line in Fig. 5(c)] display a clear enhancement of  $\omega$  as  $n$  decreases (asymmetry increases); this is consistent with our analysis.

In the following, we estimate the realistic rotational speed of the diffusiophoretic turbine with blade beads of  $1 \mu\text{m}$ . Previous experiments show that a polystyrene carboxylate particle of radius  $0.1 \mu\text{m}$  in a solution of LiCl of concentration  $0.05 M$  has a diffusiophoretic mobility of  $D_{DP} \sim 300 \mu\text{m}^2/\text{s}$  [21]. In general,  $D_{DP}$  is size-independent in the thin Debye layer approximation [29], such that the diffusiophoretic coefficient of the  $1 \mu\text{m}$  bead is  $\alpha_D \sim 1.1 \times 10^{-4} \text{ kg } \mu\text{m}^2/\text{s}^2 M$ . Using a mapping strategy similar to the thermophoretic case, we obtain  $\omega \sim 1.2 \text{ Rad/s}$ . On the other hand, from the dimensional argument, the rotational speed is estimated as  $\omega \simeq \delta \alpha_D \nabla c / 4\pi \eta \sigma^2 \sim 0.9 \text{ Rad/s}$ , under a moderate concentration gradient  $\nabla c \sim 5 \times 10^{-4} M/\mu\text{m}$ . Thus, the mapped angular velocity from the simulation agrees with that obtained from the dimensional argument.

#### IV. DISCUSSION

The proposed phoretic microturbines are fundamentally different from existing active microrotors. The driving fields or key ingredients for the motion of active microrotors are usually generated locally by the self-propelling elements on the rotor, even in the presence of an applied external field [32,55–57]. The individual blade of the active microrotors self-propels along its intrinsic symmetric axis, regardless of the orientation of the external field. Our microturbines, however, are passive devices that are directly driven by externally existing gradient fields. The blade of our microturbines exhibits passive phoresis instead of self-phoresis.

As a proof of concept, the estimated rotational speeds of our turbines are sufficient for possible applications in microfluidics, with large room for technical improvements. For instance, the angular velocity of turbines operating at a gas-liquid interface can increase by orders of magnitude larger via diffusiocapillary or thermocapillary effects [58], and the selection or development of materials with a giant phoretic factor [59] can significantly improve the turbine performance. Moreover, due to the temperature (concentration) dependence of phoretic factors [35–39], the anisotropy of the blade phoresis is expected to be dependent on temperature (or concentration). These dependencies provide additional degrees of freedom to optimize and tune the performance of the phoretic turbines.

The phoretic microturbines we propose can be fabricated using colloidal synthesis and assembly techniques. For instance, a Janus particle with fore-and-aft nonsymmetric phoresis is a natural choice for the blades of microturbines. Thus, rigid doublets or triplets of Janus particles may constitute a simple microturbine; these are

often formed spontaneously during the manufacturing of Janus particles [32,56]. The assembly of microturbines can also be directed by optical tweezers; the bonds between particles are created by UV-activated reactions. Another route to prepare microturbines is to take advantage of state-of-the-art micro- or nanofabrication techniques, including laser direct writing, focused ion beam, or photolithography, together with metal deposition [57]. These micro- or nanofabrication techniques can create complex shapes with high precision. The required fore-and-aft nonsymmetric phoretic property of each blade can be realized either by geometry alone, which greatly reduces the engineering complexity, or by selective deposition. A freely moving turbine may still drift parallel to the gradient from the non-vanishing phoresis of the whole turbine. The turbine can be pinned by an external axis through the center, fabricated using the laser direct writing technique, or by optical or magnetic tweezers. In the case of ac-type gradient fields, no pinning is needed to maintain unidirectional rotation of the microturbines with a vanishing average drift.

Finally, we discuss potential applications of the phoretic turbines. Passive microturbines driven by external gradients can extract useful work directly from waste heat or chemical diffusion. This is in contrast to existing self-phoretic active rotors that require spending “fuel” to create local gradients for propulsion; hence, these rotors cannot recycle waste energy carried by external diffusive fluxes. Specifically, a phoretic microturbine with magnetic material rotating in diffusive fluxes can generate electric power due to induction. Such energy harvested on a small scales can be used to power microdevices connected to the turbine, e.g., artificial flagella, which is reminiscent of the rotary motor of bacterial flagella. It is unlikely, however, to be a solution to macroscopic energy needs. Another possible application of these turbines is as a stirring device. A diffusiophoretic turbine can mix multiple components in the presence of chemical inhomogeneity (microfluidic mixer); a thermophoretic turbine can facilitate heat conduction in the presence of thermal inhomogeneity. When the turbine is asymmetrically pinned in a microchannel, due to asymmetric hydrodynamic interactions with the channel boundaries, the rotational turbine can generate a net fluid flow through the channel, which is a microfluidic pump. On the other hand, when turbine rotation is externally constrained, the nonvanishing phoretic torque can produce a quasi-long-range rotational flow field around the turbine, constituting a rotational pump.

#### V. CONCLUSIONS

We show that an external diffusive heat or mass flow can drive a microturbine to rotate perpendicular to the flow direction by performing mesoscale dynamics simulations. The driving mechanism is based on fore-and-aft asymmetric phoresis. The performance of the phoretic turbine thus

requires no aligning operation. This scenario is reminiscent of Darrieus-type turbines driven by external convective flows, but with essentially different physics. The present work is an important complement to previously proposed prototype phoretic turbines that rotate parallel to the external gradients [10,11]. Therefore, the perpendicular-axis phoretic turbines enrich external gradient-driven micro-machines, and suggest the possibility to exploit otherwise wasted energy carried in diffusive fluxes that are ubiquitous on the microscale.

## ACKNOWLEDGMENTS

We acknowledge financial support from the NSFC (Grants No. 11874397, No. 11674365, No. 11474327, and No. 11774393). This work was also supported by the MOST 973 Program (Grant No. 2015CB856800).

- [1] P. Galajda and P. Ormos, Complex micromachines produced and driven by light, *Appl. Phys. Lett.* **78**, 249 (2001).
- [2] R. Di Leonardo, A. Búzás, L. Kelemen, G. Vizsnyiczai, L. Oroszi, and P. Ormos, Hydrodynamic Synchronization of Light Driven Microrotors, *Phys. Rev. Lett.* **109**, 034104 (2012).
- [3] Y. Zong, J. Liu, R. Liu, H. Guo, M. Yang, Z. Li, and K. Chen, An optically driven bistable Janus rotor with patterned metal coatings, *ACS Nano* **9**, 10844 (2015).
- [4] S. Bianchi, G. Vizsnyiczai, S. Ferretti, C. Maggi, and R. Di Leonardo, An optical reaction micro-turbine, *Nat. Commun.* **9**, 4476 (2018).
- [5] J. L. Anderson, Colloid transport by interfacial forces, *Annu. Rev. Fluid Mech.* **21**, 61 (1989).
- [6] R. Piazza and A. Parola, Thermophoresis in colloidal suspensions, *J. Phys.: Condens. Matter* **20**, 153102 (2008).
- [7] A. Würger, Thermal non-equilibrium transport in colloids, *Rep. Prog. Phys.* **73**, 126601 (2010).
- [8] B. Abécassis, C. Cottin-Bizonne, C. Ybert, A. Ajdari, and L. Bocquet, Boosting migration of large particles by solute contrasts, *Nature Mater.* **7**, 785 (2008).
- [9] D. Velegol, A. Garg, R. Guha, A. Kar, and M. Kumar, Origins of concentration gradients for diffusiophoresis, *Soft Matter* **12**, 4686 (2016).
- [10] M. Yang, R. Liu, M. Ripoll, and K. Chen, A microscale thermophoretic turbine driven by external diffusive heat flux, *Nanoscale* **6**, 13550 (2014).
- [11] M. Yang, R. Liu, M. Ripoll, and K. Chen, A microscale turbine driven by diffusive mass flux, *Lab Chip* **15**, 3912 (2015).
- [12] Z. Tan, M. Yang, and M. Ripoll, Anisotropic thermophoresis, *Soft Matter* **13**, 7283 (2017).
- [13] M. Islam, D. Ting, and A. Fartaj, Aerodynamic models for darrieus-type straight-bladed vertical axis wind turbines, *Renew. Sust. Energy Rev.* **12**, 1087 (2008).
- [14] M. R. Castelli, A. Englaro, and E. Benini, The Darrieus wind turbine: Proposal for a new performance prediction model based on CFD, *Energy* **36**, 4919 (2011).

- [15] S. Duhr and D. Braun, Why molecules move along a temperature gradient, *Proc. Natl. Acad. Sci.* **103**, 19678 (2006).
- [16] H. Ning, J. K. G. Dhont, and S. Wiegand, Thermal-diffusive behavior of a dilute solution of charged colloids, *Langmuir* **24**, 2426 (2008).
- [17] D. Stadelmaier and W. Köhler, From small molecules to high polymers: Investigation of the crossover of thermal diffusion in dilute polystyrene solutions, *Macromolecules* **41**, 6205 (2008).
- [18] H. R. Jiang, H. Wada, N. Yoshinaga, and M. Sano, Manipulation of Colloids by a Nonequilibrium Depletion Force in a Temperature Gradient, *Phys. Rev. Lett.* **102**, 208301 (2009).
- [19] J. Burelbach, D. B. Brückner, D. Frenkel, and E. Eiser, Thermophoretic forces on a mesoscopic scale, *Soft Matter* **14**, 7446 (2018).
- [20] D. Prieve and R. Roman, Diffusiophoresis of a rigid sphere through a viscous electrolyte solution, *J. Chem. Soc. Faraday Trans.* **83**, 1287 (1987).
- [21] J. Palacci, B. Abécassis, C. Cottin-Bizonne, C. Ybert, and L. Bocquet, Colloidal Motility and Pattern Formation under Rectified Diffusiophoresis, *Phys. Rev. Lett.* **104**, 138302 (2010).
- [22] D. C. Prieve, S. M. Malone, A. S. Khair, R. F. Stout, and M. Y. Kanj, Diffusiophoresis of charged colloidal particles in the limit of very high salinity, *Proc. Natl. Acad. Sci.* **116**, 18257 (2019).
- [23] R. P. Sear, Diffusiophoresis in Cells: A General Nonequilibrium, Nonmotor Mechanism for the Metabolism-dependent Transport of Particles in Cells, *Phys. Rev. Lett.* **122**, 128101 (2019).
- [24] D. Vigolo, R. Rusconi, H. A. Stone, and R. Piazza, Thermophoresis: Microfluidics characterization and separation, *Soft Matter* **6**, 3489 (2010).
- [25] L. Lin, X. Peng, X. Wei, Z. Mao, C. Xie, and Y. Zheng, Thermophoretic tweezers for low-power and versatile manipulation of biological cells, *ACS Nano* **11**, 3147 (2017).
- [26] E. L. Talbot, J. Kotar, L. Parolini, L. Di Michele, and P. Cicuta, Thermophoretic migration of vesicles depends on mean temperature and head group chemistry, *Nat. Commun.* **8**, 15351 (2017).
- [27] D. Niether, D. Afanasenkov, J. K. G. Dhont, and S. Wiegand, Accumulation of formamide in hydrothermal pores to form prebiotic nucleobases, *Proc. Natl. Acad. Sci.* **113**, 4272 (2016).
- [28] T. Tsuji, S. Saita, and S. Kawano, Dynamic Pattern Formation of Microparticles in a Uniform Flow by an On-chip Thermophoretic Separation Device, *Phys. Rev. Appl.* **9**, 024035 (2018).
- [29] S. Shin, E. Um, B. Sabass, J. T. Ault, M. Rahimi, P. B. Warren, and H. A. Stone, Size-dependent control of colloid transport via solute gradients in dead-end channels, *Proc. Natl. Acad. Sci.* **113**, 257 (2016).
- [30] S. Shin, J. T. Ault, P. B. Warren, and H. A. Stone, Accumulation of Colloidal Particles in Flow Junctions Induced by Fluid Flow and Diffusiophoresis, *Phys. Rev. X* **7**, 041038 (2017).
- [31] J. R. Howse, R. A. L. Jones, A. J. Ryan, T. Gough, R. Vafabakhsh, and R. Golestanian, Self-motile Colloidal Particles, *Phys. Rev. Lett.* **99**, 048102 (2007).

- [32] H. R. Jiang, N. Yoshinaga, and M. Sano, Active Motion of a Janus Particle by Self-thermophoresis, *Phys. Rev. Lett.* **105**, 268302 (2010).
- [33] M. Xuan, Z. Wu, J. Shao, L. Dai, T. Si, and Q. He, Near infrared light-powered janus mesoporous silica nanoparticle motors, *J. Am. Chem. Soc.* **138**, 6492 (2016).
- [34] E. Lattuada, S. Buzzaccaro, and R. Piazza, Thermophoresis in self-associating systems: Probing poloxamer micellization by opto-thermal excitation, *Soft Matter* **15**, 2140 (2019).
- [35] N. Shi, R. Nery-Azevedo, A. I. Abdel-Fattah, and T. M. Squires, Diffusiophoretic Focusing of Suspended Colloids, *Phys. Rev. Lett.* **117**, 258001 (2016).
- [36] A. Würger, Transport in Charged Colloids Driven by Thermoelectricity, *Phys. Rev. Lett.* **101**, 108302 (2008).
- [37] D. Vigolo, S. Buzzaccaro, and R. Piazza, Thermophoresis and thermoelectricity in surfactant solutions, *Langmuir* **26**, 7792 (2010).
- [38] S. A. Putnam, D. G. Cahill, and G. C. L. Wong, Temperature dependence of thermodiffusion in aqueous suspensions of charged nanoparticles, *Langmuir* **23**, 9221 (2007).
- [39] M. Braibanti, D. Vigolo, and R. Piazza, Does Thermophoretic Mobility Depend on Particle Size? *Phys. Rev. Lett.* **100**, 108303 (2008).
- [40] A. Malevanets and R. Kapral, Mesoscopic model for solvent dynamics, *J. Chem. Phys.* **110**, 8605 (1999).
- [41] J. T. Padding and A. A. Louis, Hydrodynamic interactions and brownian forces in colloidal suspensions: Coarse-graining over time and length-scales, *Phys. Rev. E* **93**, 031402 (2006).
- [42] R. Kapral, Multiparticle collision dynamics: Simulation of complex systems on mesoscales, *Adv. Chem. Phys.* **140**, 89 (2008).
- [43] G. Gompper, T. Ihle, D. M. Kroll, and R. G. Winkler, Multiparticle collision dynamics: A particle-based mesoscale simulation approach to the hydrodynamics of complex fluids, *Adv. Polym. Sci.* **221**, 1 (2009).
- [44] J. F. Ryder, Mesoscopic simulations of complex fluids, Ph.D. thesis, University of Oxford, 2005.
- [45] A. Lamura, G. Gompper, T. Ihle, and D. M. Kroll, Multiparticle collision dynamics: Flow around a circular and a square cylinder, *Europhys. Lett.* **56**, 319 (2001).
- [46] F. Müller-Plathe, A simple nonequilibrium molecular dynamics method for calculating the thermal conductivity, *J. Chem. Phys.* **106**, 6082 (1997).
- [47] D. Lüsebrink and M. Ripoll, Temperature inhomogeneities simulated with multiparticle-collision dynamics, *J. Chem. Phys.* **136**, 084106 (2012).
- [48] M. Yang and M. Ripoll, Thermophoretically induced flow field around a colloidal particle, *Soft Matter* **9**, 4661 (2013).
- [49] F. Römer, F. Bresme, J. Muscatello, D. Bedeaux, and J. M. Rubí, Thermomolecular Orientation of Nonpolar Fluids, *Phys. Rev. Lett.* **108**, 105901 (2012).
- [50] G. Rückner and R. Kapral, Chemically Powered Nanodimers, *Phys. Rev. Lett.* **98**, 150603 (2007).
- [51] M. Yang, A. Wysocki, and M. Ripoll, Hydrodynamic simulations of self-phoretic microswimmers, *Soft Matter* **10**, 6208 (2014).
- [52] S. Iacopini, R. Rusconi, and R. Piazza, The macromolecular tourist: Universal temperature dependence of thermal diffusion in aqueous colloidal suspensions, *Eur. Phys. J. E* **19**, 59 (2006).
- [53] M. Yang and M. Ripoll, Simulations of thermophoretic nanoswimmers, *Phys. Rev. E* **84**, 061401 (2011).
- [54] M. Yang and M. Ripoll, Thermoosmotic microfluidics, *Soft Matter* **12**, 8564 (2016).
- [55] S. Ebbens, R. A. L. Jones, A. J. Ryan, R. Golestanian, and J. R. Howse, Self-assembled autonomous runners and tumblers, *Phys. Rev. E* **82**, 015304(R) (2010).
- [56] A. Boymelgreen, G. Yossifon, S. Park, and T. Miloh, Spinning janus doublets driven in uniform ac electric fields, *Phys. Rev. E* **89**, 011103 (2014).
- [57] C. W. Shields IV, K. Han, F. Ma, T. Miloh, G. Yossifon, and O. D. Velev, Supercolloidal spinners: Complex active particles for electrically powered and switchable rotation, *Adv. Funct. Mater.* **28**, 1803465 (2018).
- [58] C. Maggi, F. Saglimbeni, M. Dipalo, F. De Angelis, and R. Di Leonardo, Micromotors with asymmetric shape that efficiently convert light into work by thermocapillary effects, *Nat. Commun.* **6**, 7855 (2015).
- [59] S. Wongswarn, D. Vigolo, R. Cerbino, A. M. Howe, A. Vailati, R. Piazza, and P. Cicuta, Giant thermophoresis of poly(n-isopropylacrylamide) microgel particles, *Soft Matter* **8**, 5857 (2012).